RP Current Trends In Applied Sciences (e-ISSN: 2583-7486)
Vol. 5, No. 1 (January – March 2026) pp. 42–47

RESEARCH PLATEAU PUBLISHERS

Cite this article: P.K. Vishwakarma, C. Kumari, Red emitting Eu^{3+} doped $SrNb_2O_6$ phosphors: Structural and luminescence studies, *RP Cur. Tr. Appl. Sci.* **5** (2026) 42–47.

Original Research Article

Red emitting Eu^{3+} doped $SrNb_2O_6$ phosphors: Structural and luminescence studies

Praveen Kumar Vishwakarma[1,*], Chandni Kumari[2]

[1]Department of Physics, Patna University, Patna, Bihar - 800005, India
[2]Department of Physics, IIT (ISM), Dhanbad, Jharkhand - 826004, India
*Corresponding author, E-mail: pk31825@gmail.com

ARTICLE HISTORY
Received: 15 April 2026
Revised: 27 May 2026
Accepted: 27 May 2026
Published: 12 June 2026

KEYWORDS
Solid-state method;
Diffuse reflectance spectra;
Burstein – Moss effect;
Photoluminescence;
Concentration quenching.

ABSTRACT
Intense red-emitting double perovskite $SrNb_2O_6$ (SNO) phosphors were successfully synthesized through a conventional solid-state reaction method with Europium (Eu^{3+}) as the activator. Structural analysis confirmed that the synthesized samples possess a hexagonal crystal system with the p21/c space group. FTIR spectra revealed the various functional group present in the samples. Diffuse reflectance measurements indicated that the optical band gap of SNO doped with 4 mol% Eu^{3+} is approximately 3.96 eV, slightly lower than that of the undoped host (3.93 eV), suggesting the occurrence of the Burstein - Moss effect. Photoluminescence studies revealed strong red emission, with an optimal dopant concentration of 4 mol% Eu^{3+}. Beyond this concentration, emission intensity decreases due to concentration quenching, which is attributed to dipole - dipole interactions among Eu^{3+} ions. The luminescence decay analysis yielded an average lifetime of 808.6 µs. Photometric evaluation demonstrated low correlated color temperature (CCT < 1900 K), high color purity (≈ 99%), and Commission Internationale de l'Éclairage (CIE) chromaticity coordinates located in the red region. These results indicate that the developed phosphor is a promising candidate for application in white light - emitting diodes (wLEDs) based on ultraviolet or blue excitation sources.

1. Introduction

In recent years, phosphor-converted white light-emitting diodes (pc-WLEDs) have attracted significant research interest due to their low power consumption, long operational lifetime, environmental friendliness, and rapid response [1,2]. Conventionally, white light generation is achieved by combining a blue LED chip with a yellow-emitting phosphor. However, this approach suffers from inherent limitations such as a low color rendering index (CRI) and high correlated color temperature (CCT), primarily due to the insufficient red spectral component. To address these issues, an alternative strategy involving near-ultraviolet (n-UV) LED chips coupled with red, green, and blue phosphors has been developed, enabling improved color quality and tunable warm white light emission [3,4].

Among various luminescent materials, rare-earth (lanthanide) ions have gained considerable attention owing to their outstanding optical properties, including high photostability, sharp emission lines, and wide spectral coverage ranging from the ultraviolet to the near-infrared region [5,6]. These ions possess rich energy level structures, facilitating efficient radiative transitions such as Stokes and anti-Stokes processes. Moreover, the shielding of 4f electrons by outer 5s and 5p orbitals minimizes the influence of the host lattice, resulting in stable and host-independent emission characteristics [6]. These unique features make rare-earth-doped phosphors highly suitable for applications in solid-state lighting, displays, bioimaging, security inks, and anti-counterfeiting technologies [5].

In particular, trivalent Europium (Eu^{3+}) is recognized as one of the most efficient activator ions for red emission, owing to its characteristic intra - 4f transitions. The dominant emissions originate from the $^5D_0 \rightarrow {}^7F_1$ transition (orange emission around 589 nm) and the hypersensitive $^5D_0 \rightarrow {}^7F_2$ transition (intense red emission in the 612–624 nm range) [7,8].

Various oxide-based host lattices, including tungstates, molybdates, vanadates, phosphates, and silicates, have been extensively explored due to their excellent chemical stability and ability to efficiently absorb UV radiation and transfer energy to activator ions [8–12]. For instance, Eu^{3+} - doped $SrWO_4$ [8], $CaMoO_4$ [9], $La_{1-x}Eu_xCoO_3$ [13] and related oxide hosts have demonstrated promising red emission characteristics.

Recently, niobate-based host materials, particularly $SrNb_2O_6$, have emerged as attractive candidates due to their structural stability, favorable optical properties, and efficient energy transfer mechanisms. Despite these advantages, systematic investigations on Eu^{3+} - activated $SrNb_2O_6$ (SNO) phosphors for red emission and their applicability in solid-state lighting remain limited. Therefore, in the present work, Eu^{3+} - doped $SrNb_2O_6$ phosphors are investigated in detail to explore their structural and photoluminescence properties, aiming to develop an efficient red-emitting material for white light-emitting diode applications.

2. Experimental process

A series of $SrNb_2O_6$ phosphors doped with Europium (Eu^{3+}) at varying concentrations were synthesized using a conventional solid-state reaction technique. Stoichiometric amounts of $SrCO_3$, Nb_2O_5, and europium oxide (Eu_2O_3) were accurately weighed according to their molar ratios. The precursors were thoroughly homogenized in an ethanol medium using an agate mortar and pestle for approximately 2 hours to ensure uniform mixing. The resulting mixture was then transferred into an alumina crucible and calcined in a muffle furnace at 1250 °C for 7 hours. The heating and cooling rates were carefully controlled at 5 °C per minute during the temperature ramp-up and ramp-down processes. After completion of the heat treatment, the samples were allowed to cool naturally to room temperature, removed from the furnace, and subsequently ground into fine powders for further characterization.

3. Characterization techniques

The crystallinity and phase purity of the synthesized samples were examined using a high-resolution X-ray diffractometer (Rigaku) equipped with Cu-K_α radiation (λ = 1.5418 Å). Fourier transform infrared (FTIR) spectra were recorded in the range of 400 - 4000 cm^{-1} using an INVENIO S spectrometer (Bruker Optik GmbH). Diffuse reflectance spectra (DRS) were recorded using a UV - Vis - NIR spectrophotometer (Model 5000) equipped with an integrating sphere to ensure accurate diffuse reflectance measurements. The photoluminescence (PL) properties were investigated using an Agilent Cary Eclipse equipped with a xenon lamp as the excitation source. Furthermore, photometric parameters such as Commission Internationale de l'Éclairage (CIE) chromaticity coordinates, correlated color temperature (CCT), and color purity were evaluated using software tools including ColorCalculator and GoCIE.

4. Results and Discussion

4.1 Structural investigation

4.1.1 XRD analysis

Figure 1 illustrates the powder X-ray diffraction (PXRD) pattern of $SrNb_2O_6$ doped with 1 mol% Europium (Eu^{3+}). All the observed diffraction peaks are in good agreement with the standard data (JCPDS card no. 00-028-1248), confirming the successful formation of a single-phase material without any detectable impurity or secondary phases. This indicates that the Eu^{3+} ions are effectively incorporated into the host lattice without significantly altering its crystal structure. The diffraction analysis reveals that the synthesized sample crystallizes in a monoclinic crystal system.

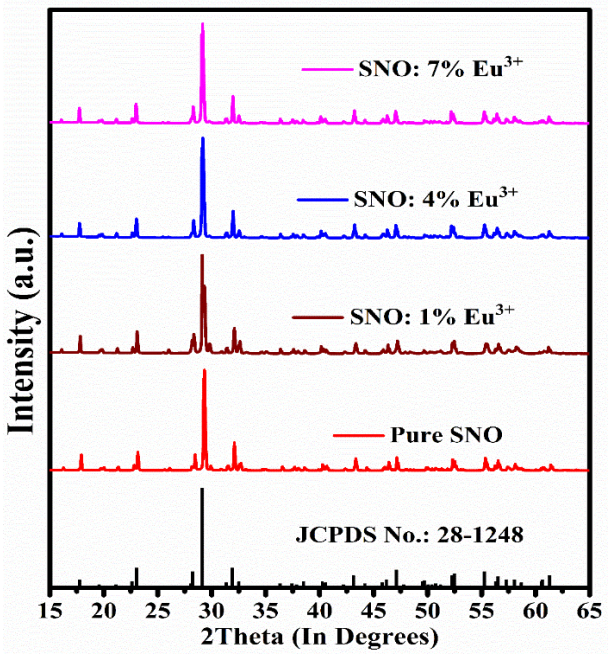

Figure 1: XRD patterns of $SrNb_2O_6$: xEu^{3+} (x = 0, 0.01, 0.04, and 0.07) samples.

In addition, the average crystallite size of the prepared phosphor was estimated using the Debye - Scherrer equation, which relates the broadening of diffraction peaks to the size of coherently diffracting domains. This method provides a useful approximation of the nanocrystalline nature of the synthesized material. The Debye - Scherrer equation is expressed as follows [14]:

$$D = \frac{0.9\lambda}{\gamma \cos\theta}$$

In this equation, D represents the average crystallite size, while γ corresponds to the full width at half maximum (FWHM) of the diffraction peak, θ is angle of diffraction and λ denotes the wavelength of the incident X-ray radiation. Table 1 shows the crystallite size and volume of the doped and undoped samples.

Table 1: Crystallite size, lattice constants and cell volume of $SrNb_2O_6$: xEu^{3+} (x = 0, 0.01, 0.04, and 0.07) samples.

Eu^{3+} Concentration (mol %)	Average Crystallite Size (nm)	Lattice constants (Å)			Cell Volume ($Å^3$)
		a	*b*	*c*	
0	43	7.716	5.595	10.998	474.663
1	47	7.726	5.594	10.992	475.201
4	48	7.720	5.590	10.995	474.629
7	42	7.719	5.591	10.999	475.098

Table 2: Chromaticity coordinates (*x*, *y*), CCT and Color Purity (CP) of SNO: Eu^{3+} phosphors at different Eu^{3+} concentrations.

Eu^{3+} concentrations (mol%)	Chromaticity Coordinates		CCT(K)	Color Purity (%)
	x	*y*		
1	0.6305	0.3604	2132	97.4
4	0.6372	0.3596	2211	99.2
6	0.6408	0.3578	2281	99.7
7	0.6397	0.3584	2258	99.5

4.1.2 FTIR analysis

Figure 2 shows the FTIR spectra of pure and Europium (Eu^{3+}) - doped $SrNb_2O_6$ phosphors in the range of 400 – 4000 cm^{-1}. The bands at 417 and 540 cm^{-1} are attributed to Nb – O and O – Nb – O vibrations, confirming the formation of the NbO_6 framework [15]. Additional bands at 759 and 837 cm^{-1} arise from lattice vibrations of Nb – O bonds. The peaks at 1211 and 1367 cm^{-1} correspond to carbonate (CO_3^{2-}) groups, while the band at 1736 cm^{-1} is assigned to C = O stretching vibrations. The absorption band at 1736 cm^{-1} is assigned to C = O stretching vibrations, indicating the presence of carbonyl groups, possibly due to adsorbed CO_2 or incomplete decomposition of carbonate species [16,17]. The absorption at 3020 cm^{-1} is due to C – H stretching, and the band at 3734 cm^{-1} is related to O – H vibrations, indicating the presence of hydroxyl groups or adsorbed moisture [17, 18].

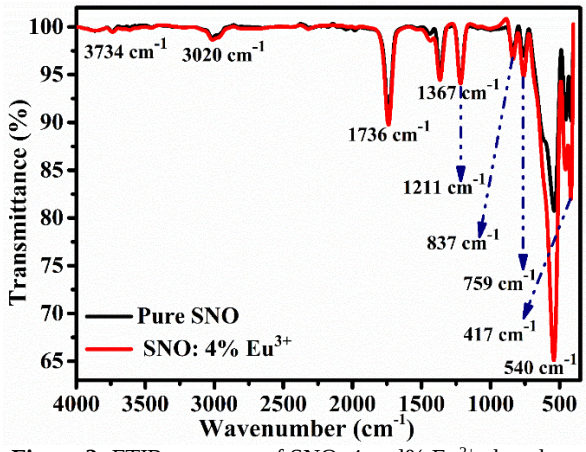

Figure 2: FTIR spectrum of SNO: 4 mol% Eu^{3+} phosphor.

4.2 Optical investigations

4.2.1 UV-Vis Diffuse Reflectance Spectra

Diffuse reflectance spectroscopy (DRS) is used to estimate the optical band gap of powdered or crystalline materials due to enhanced scattering. The reflectance is expressed as: $R_\infty = R_{sample}/R_{Reference}$. According to the Kubelka–Munk theory, the relation between absorption (K), scattering (S), and reflectance is:

$$F(R_\infty) = \frac{(1-R)^2}{2*R} = \frac{K}{S}.$$

The optical band gap is determined by Tauc relation [13]:

$$\alpha h\nu = B(h\nu - E_g)^n.$$

Assuming constant scattering, the Eqs. combine as [19]:

$$B(h\nu - E_g) = [F(R_\infty)h\nu]^{1/2}.$$

The best fit is obtained for n = 1/2 indicating a direct allowed transition. The band gap is estimated from the extrapolation of the linear region of $[F(R_\infty)h\nu]^{1/2}$ vs. $h\nu$ plot. The values of band gaps have been mentioned in the graphs itself. The decrease in band gap is attributed to the Burstein - Moss effect [20].

4.2.2 Photoluminescence studies

The photoluminescence behavior of of $SrNb_2O_6$ doped with Europium (Eu^{3+}) at different concentrations is illustrated in Fig. (a - d).

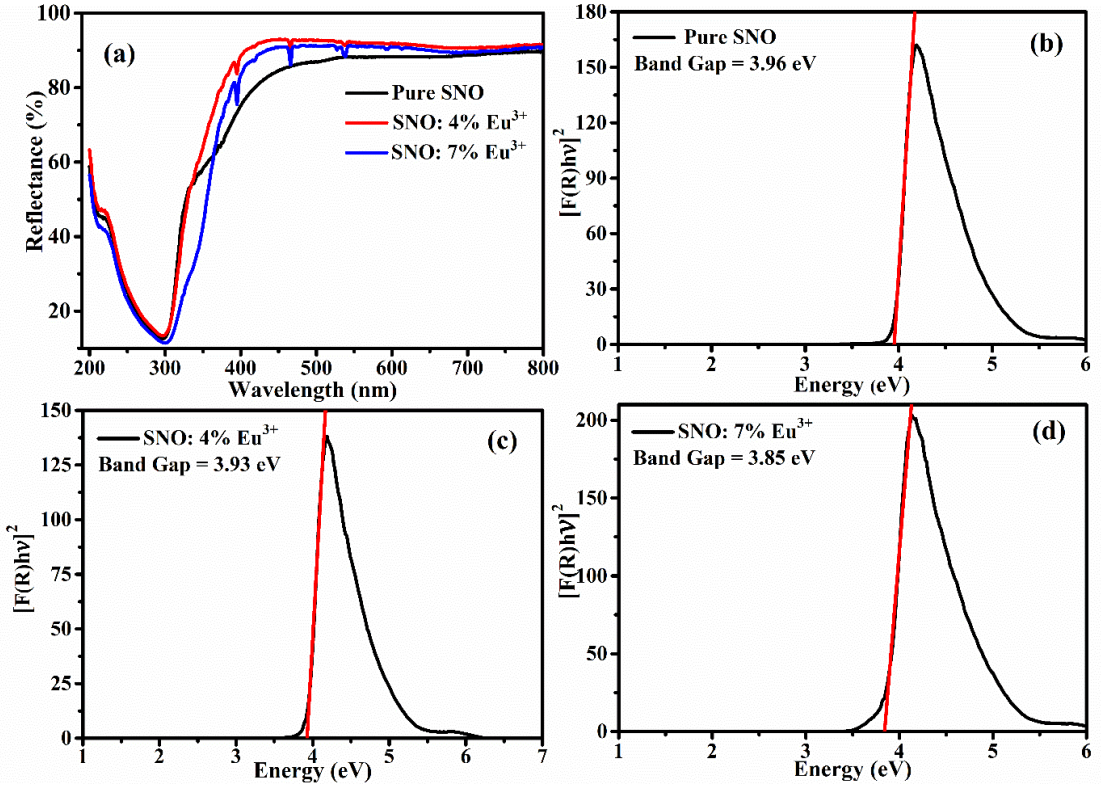

Figure 3: (a) Diffuse reflectance spectra and KM plots of (b) pure; (c) 4 mol%; (d) 7 mol%; Eu^{3+} doped SNO phosphor materials.

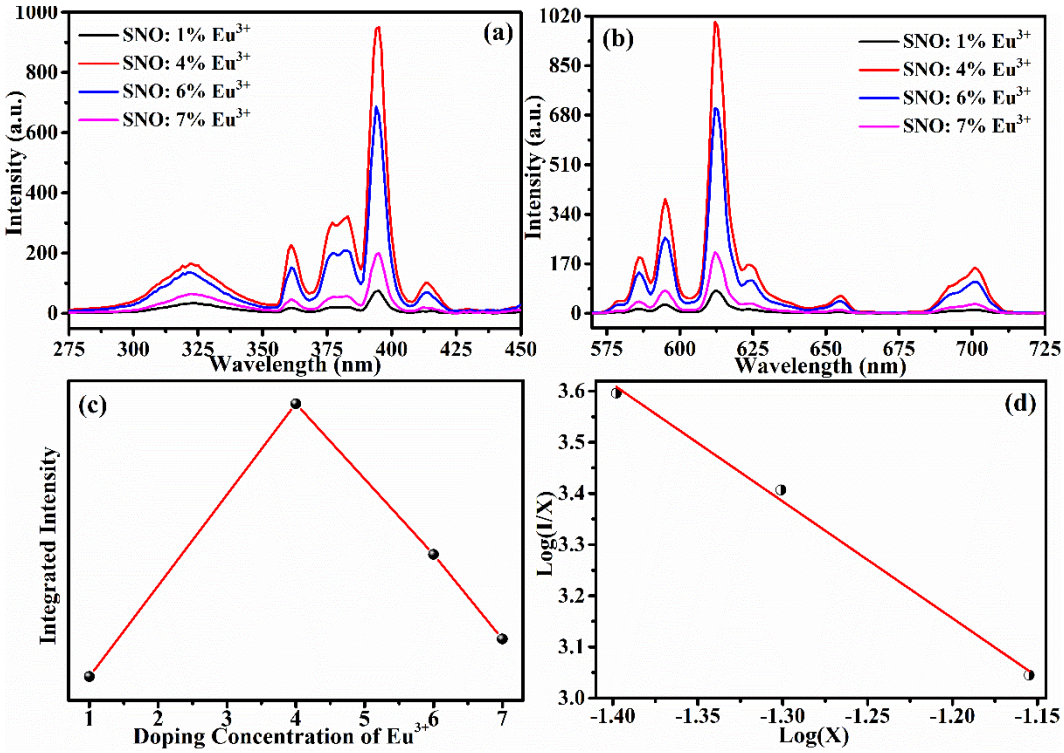

Figure 4: PL (a) Excitation spectra (λ_{emi} = 612 nm); (b) Emission spectra (λ_{exc} = 395); (c) Concentration quenching and (d) Plot of Log(X) vs. Log(I/X).

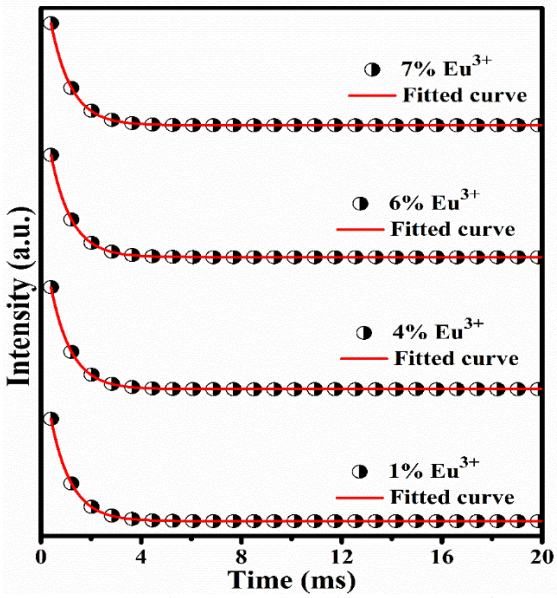

Figure 5: Decay curve recorded at λ_{exc} = 395 nm and λ_{emi} = 612 nm for SNO: Eu^{3+} phosphors.

The excitation spectrum (Fig. a) shows a broad charge transfer band in the UV region along with sharp f - f transitions of Eu^{3+}, indicating efficient absorption of UV radiation. Upon excitation, the emission spectra (Fig. b) exhibit characteristic peaks in the 570 - 725 nm region corresponding to the transitions from the $^5D_0$ excited state to the ^7F_J (J = 1, 2, 3, 4) levels of Eu^{3+}. Among these, the dominant emission is observed around ~ 612 nm ($^5D_0 \rightarrow {}^7F_2$), confirming strong red emission due to the electric dipole transition and suggesting that Eu^{3+} ions occupy non-centrosymmetric sites in the host lattice [20].

The variation of emission intensity with dopant concentration (Fig. c) shows that the intensity increases with increasing Eu^{3+} concentration and reaches a maximum at 4 mol%, followed by a decrease due to concentration quenching. The linear behavior observed in the log(I/X) versus log(X) plot (Fig. d) indicates that the quenching mechanism is governed by multipolar interactions, predominantly dipole - dipole in nature.

From an application perspective, the intense red emission, optimal doping concentration, and efficient energy transfer characteristics make $SrNb_2O_6$: Eu^{3+} phosphors promising candidates for use in phosphor-converted white light-emitting diodes (wLEDs). Their strong emission in the red region can effectively compensate for the red deficiency in conventional LED systems, thereby improving the color rendering index (CRI) and lowering the correlated color temperature (CCT). Additionally, these phosphors may find potential applications in display technologies and solid-state lighting due to their spectral stability and high color purity [13].

4.2.3 Decay kinetics

The photoluminescence decay curves of Eu^{3+} - doped $SrNb_2O_6$ were well fitted with a single exponential function, indicating a uniform luminescence center and a single dominant recombination pathway. The decay behavior follows [21]:

$$I = I_o e^{-\frac{t}{\tau}},$$

where τ is the lifetime. The obtained lifetime in the microsecond range confirms the characteristic 4f - 4f transitions of Eu^{3+} ions. Such relatively long lifetimes suggest efficient radiative recombination with minimal non-radiative losses, which is favorable for luminescent applications.

4.2.4 CIE chromaticity analysis

The Commission Internationale de l'Éclairage (CIE) chromaticity diagram shows that the emission coordinates of the $SrNb_2O_6$: Eu^{3+} phosphor lie in the deep red region. This confirms the dominance of the $^5D_o \rightarrow {}^7F_2$ transition of Europium, responsible for pure red emission. The coordinates indicate high color purity and suitability for warm white light generation when combined with other phosphors.

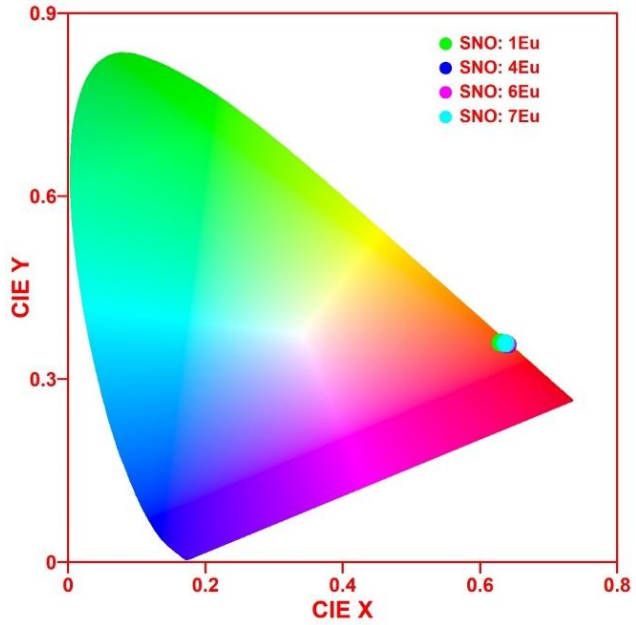

Figure 6: CIE diagrams for $SrNb_2O_6$: xEu^{3+} (x = 0.01, 0.04, 0.06 and 0.07) phosphors.

The correlated color temperature (CCT) of a phosphor represents the temperature of an ideal blackbody radiator that emits light with a color similar to that of the phosphor. In this study, the CCT values were calculated using the McCamy relation [22]:

$$CCT = -437m^3 + 3601m^2 - 6861m + 5514.31$$

where $m = \frac{x-x_e}{y-y_e}$, and x and y are the CIE color coordinates, while x_e and y_e are 0.332 and 0.186 represent the convergence epicentre, respectively. The calculated CIE coordinates, color purity, and CCT values for $SrNb_2O_6$ doped with Eu^{3+} at various concentrations were summarized accordingly in Table 2.

In general, CCT values above 4000 K correspond to cool white light suitable for commercial lighting, whereas values below 4000 K indicate warm white light, desirable for indoor and display applications [23]. The obtained CCT values lie in the low range (~2300 K), confirming the strong red emission of the phosphor and highlighting its suitability for warm white light-emitting diode applications.

5. Conclusions

Based on the structural, optical, and luminescence investigations, Eu^{3+} - doped $SrNb_2O_6$ phosphors were successfully synthesized with high phase purity, as confirmed by XRD analysis. FTIR results verified the formation of the Nb - O framework along with minor surface - related groups. UV - Vis diffuse reflectance studies indicated a direct band gap with slight variation upon doping, suggesting modification in electronic structure. Photoluminescence analysis revealed intense red emission dominated by the $^5D_o \rightarrow {}^7F_2$ transition, with an optimal doping concentration of 4 mol% due to concentration quenching effects governed by dipole -dipole interactions. The favorable decay characteristics and chromaticity coordinates in the red region further confirm that the developed phosphor is a promising candidate for red - emitting components in white light - emitting diode (wLED) applications.

Acknowledgements

The authors acknowledge the central research facility, IIT (ISM) Dhanbad.

Authors' contributions

Praveen Kumar Vishwakarma – Study conception and design, data analysis and manuscript writing.

Chandni Kumari – Sample preparation, data collection and analysis.

The author read and approved the final manuscript.

Conflicts of interest

The authors do not have any financial interest or personal relationship that can influence this work.

Funding

This research received no external funding.

Data availability

The data are presented in the manuscript.

References

[1] E.F. Schubert, J.K. Kim, Solid-state light sources getting smart, *Science* **308** (2005) 1274–1278.

[2] S. Nakamura, T. Mukai, M. Senoh, Candela-class high-brightness InGaN/AlGaN double-heterostructure blue-light-emitting diodes, *Appl. Phys. Lett*. **64** (1994) 1687–1689.

[3] B. Yang, Z. Yang, Y. Liu, F. Lu, P. Li, Y. Yang, X. Li, Luminescence properties of rare-earth doped phosphors, *Ceram. Int*. **38** (2012) 4895–4900.

[4] J. He, Q.Z. Cai, F. Xiao, X.W. Li, W. Sun, X. Zhao, Structural and luminescent properties of phosphor materials, *J. Alloys Compd*. **509** (2011) L11–L14.

[5] G. Blasse, B.C. Grabmaier, Luminescent Materials, Springer, Berlin Heidelberg (1994).

[6] N.J. English, M.M. El-Hendawy, D.A. Mooney, J.M.D. MacElroy, Coordination chemistry and luminescence behaviour of rare-earth compounds, *Coord. Chem. Rev*. **269** (2014) 85–129.
[7] J.F. Rusling, Luminescence in electrochemical systems, *Electrochem. Soc. Interface* **18** (2009) 34–38.
[8] B.P. Singh, J. Singh, R.A. Singh, Luminescence studies of phosphor compounds, *RSC Adv*. (2014).
[9] X. Zhao, N. E., X. Wang, Optical and luminescence behaviour of rare-earth activated materials, *Luminescence* **37** (2022) 1446–1453.
[10] Luminescence and the Solid State, 2nd edn. (n.d.).
[11] P. Dorenbos, Energy of the first 4f7→4f65d transition of Eu2+ in inorganic compounds, *J. Lumin*. **104** (2003) 239–260.
[12] W.M. Yen, S. Shionoya, H. Yamamoto, Phosphor Handbook, CRC Press/Taylor & Francis (2007).
[13] S. Yadav, D. Kumar, R.S. Yadav, S.B. Rai, A.K. Singh, Structural and luminescence investigations of phosphor materials, *Ceram. Int*. **48** (2022) 30754–30763.
[14] P.K. Vishwakarma, C. Kumari, Luminescent behaviour of inorganic phosphors, *Ceram. Int*. (2026).
[15] K. Nakamoto, Infrared and Raman Spectra of Inorganic and Coordination Compounds, Wiley (2008).
[16] J. Coates, Interpretation of infrared spectra, a practical approach, in: Encyclopedia of Analytical Chemistry, Wiley (2000).
[17] J.M. Chalmers, P.R. Griffiths (Eds.), Handbook of Vibrational Spectroscopy, Wiley (2001).
[18] B.H. Stuart, Infrared Spectroscopy: Fundamentals and Applications, Wiley (2004).
[19] D. Kumar, S. Yadav, C.B. Singh, R.S. Yadav, S.B. Rai, A.K. Singh, Structural and photoluminescence studies of phosphor materials, *J. Alloys Compd*. **945** (2023) 169240.
[20] C. Kumari, J. Manam, S.K. Sharma, Structural, thermal and optical properties of phosphor materials, *Mater. Sci. Semicond. Process*. **158** (2023) 107363.
[21] C. Kumari, J. Manam, S.K. Sharma, Optical and luminescence properties of rare-earth activated phosphors, *J. Mater. Sci*. **60** (2025) 11311–11325.
[22] C. Kumari, J. Manam, S.K. Sharma, Luminescence properties of rare-earth doped phosphors, *J. Lumin*. **263** (2023) 120091.
[23] K. Mondal, P. Kumari, J. Manam, Structural and optical studies of phosphor materials, *Curr. Appl. Phys*. **16** (2016) 707–713.